Study of deformation mechanisms in flash-sintered yttria-stabilized zirconia by *in-situ* micromechanical testing at elevated temperatures

Jaehun Cho[a], Jin Li[a], Han Wang[a], Qiang Li[a], Zhe Fan[b], A. K. Mukherjee[c], Haiyan Wang[a, d], and X. Zhang[a, *]

[a]School of Materials Engineering, Purdue University, West Lafayette, IN 47907, USA
[b]Oak Ridge National Laboratory, Oak Ridge, TN 37830, USA
[c]Department of Chemical Engineering & Materials Science, University of California, Davis, CA 95616, USA
[d]School of Electrical and Computer Engineering, Purdue University, West Lafayette, IN 47907, USA
*Corresponding author: xzhang98@purdue.edu

ABSTRACT

Flash sintering has received wide attention lately due to its ultrafast densification process at low sintering temperature. However, the deformability of flash-sintered ceramics remains poorly understood. Yttria-stabilized zirconia (YSZ) was processed by flash sintering to study deformation mechanism. Transmission electron microscopy studies show that the flash-sintered YSZ contains ultrafine grains and dislocations. Strain rate jump tests at elevated temperature by *in-situ* microcompression test indicate the existence of a large threshold stress. The activation energy of deformation is ~145 kJ/mol, similar to the activation energy for oxygen vacancy migration. The deformation mechanisms of the flash-sintered YSZ at elevated temperatures are discussed.

KEYWORDS

flash sintering, deformation mechanism, *in-situ* microcompression test, dislocation

IMPACT STATEMENT

The current study reveals the underlying deformation mechanisms of flash-sintered 3YSZ that shows considerable plasticity over the temperature range of 450 ~ 650^{o}C via *in-situ* microcompression test.

1. Introduction

Field-assisted sintering technique (FAST) is of great industrial importance and widely applied due to a significant energy saving by lowering sintering temperature and time [1]. Flash sintering, one of the FASTs, is a newly developed technique that permits the dramatic reduction of sintering time and temperature and permits substantial currents to flow through specimens [2]. During flash sintering, an ultrafast densification process occurs by applying an electrical field at a constant heating rate. When the furnace temperature is higher than the onset (flash) point, which is dependent upon the magnitude of applied electric field, an instantaneous densification process takes place within a few seconds [3]. Many ceramic systems, such as yttria-stabilized zirconia (YSZ), titania, zinc oxide, and ceria have been successfully prepared by flash-sintering [4–7], and the number of flash-sintered ceramic systems increases rapidly. Among these systems, YSZ is one of the most widely explored ceramics in the field of flash sintering, as YSZ has a variety of important industrial applications, such as thermal barrier coatings, dental implants, oxygen sensors, and solid oxide fuel cells [8–11].

Mechanical behavior of YSZ has been intensively investigated. Among these there are several studies on microscale mechanical testing, which mostly highlight superior superelasticity and shape memory effect at room temperature owing to martensitic transformation [12–18]. However, our understanding on deformation mechanisms of microscale YSZ at elevated temperatures remains limited. In addition, ceramics processed by flash sintering technique is

known to have intriguing microstructures containing a considerable number of charged defects and ultrafine grain sizes [3,19]. Our previous *in-situ* study shows that the flash-sintered YSZ has a high-density of preexisting dislocations induced by flash sintering and has a transition of deformation mechanisms at 400^{o}C [20]. Here, we report further studies on underlying deformation mechanism of the flash-sintered 3 mol % yttria doped zirconia (3YSZ) at elevated temperature (above 400^{o}C). We utilize *in-situ* microcompression jump tests to avoid complicated data analyses associated with nanoindentation [21]. These tests reveal the existence of a large threshold stress for activation of dislocation creep. Furthermore, the activation energy for creep is measured from *in-situ* compression tests and provides important insight on defect dominated deformation mechanisms in flash-sintered ceramics.

2. Experimental procedures

The experiment was conducted in a customized thermomechanical analyzer (SETSYS Evolution, SET ARAM Instrumentation). Disk-shaped 3YSZ specimens with a diameter of ~ 5 mm and a thickness of ~ 2 mm (using TZ-3Y-E powders, from Tosoh corp., with 40 nm grain size, please see Table S1 for purity information.) were sandwiched between two Pt electrodes and an alumina rod pushed the electrodes with a few kPa pressure to insure a rigid contact between the sample and electrodes. A compact specimen dimension was intentionally used to minimize density and grain size fluctuations throughout the sample. An electrical field of 150 V/cm was applied to the specimen with a constant heating rate of 25 ^{o}C/min until the sample undergoes a rapid densification at a furnace temperature of 1150^{o}C. Right after the onset of flash, the applied heat and electrical field were removed right away to prohibit grain growth.

Transmission electron microscopy (TEM) studies were performed on the as-sintered 3YSZ. Sequential grinding, polishing, dimpling and ion milling (PIPS II, Gatan) were employed to manually prepare TEM specimens of the flash-sintered 3YSZ. TEM experiment were performed on an FEI Talos 200X transmission electron microscope operated at 200 kV.

To investigate the microscale mechanical behavior of flash-sintered 3YSZ, micropillars with ~ 3 μm in diameter and ~ 8 μm in height were fabricated by focused ion beam (FIB) technique in an FEI 3D FEG scanning electron microscope. The pillars were prepared on a dense area (judged by SEM studies) and thus the pillars from this region contain only a few nanovoids. The specimen was mounted on a ceramic stage heater in a Hysitron PI 88×R nanoindentation system. A 5 μm diameter diamond flat punch tip equipped on a piezoelectric transducer for collection of force and displacement was used to compress the micropillars. The diamond flat punch and specimen were heated to desired temperature (450, 550, and 650 ^{o}C) at the same ramping rate of 20 ^{o}C/min. The microcompression tests were conducted when thermal equilibrium is achieved to minimize mechanical and thermal drifts. Thermal drift rate, less than 1.1 nm/s, was measured prior to each compression tests for 40 s. True displacement data compensating the displacement offset were acquired by the nanoindentation system.

3. Results

TEM micrograph (Figure 1(a)) shows ultrafine grain size in the flash-sintered 3YSZ. A systematic grain intercept method reveals the average grain size of 159 ± 70 nm with a large variation, and the flash-sintered 3YSZ has a 98% density. TEM studies also show a significant amount of preexisting dislocations (Figure 1(b)). Strain rate jump tests were carried out on numerous micropillars at different temperatures (450, 550, and 650 ^{o}C) to study the underlying deformation mechanisms. A strain rate of 5×10^{-4} s^{-1} was applied in the elastic region (~ 2%) of the

stress-strain curve, and strain rates of 3×10^{-3} s^{-1}, 1×10^{-2} s^{-1}, 5×10^{-2} s^{-1}, and 3×10^{-1} s^{-1} were applied in the plastic deformation region to obtain flow stresses at each temperature. Figure 1 (c-e) shows SEM snapshots of the tested pillars at various strains at each temperature. Cracks propagated downwards from top surface, but no catastrophic failure was observed after tests at elevated temperatures. Figure 2 (a-c) shows multiple stress-strain curves of strain rate jump tests at three temperatures. The stress-strain behavior shows good reproducibility taking into consideration the porous nature of ceramic materials. As test temperature increases, the flow stresses tend to decrease, and crack density and propagation speed reduce significantly. The flow stresses for each strain rate were obtained at a strain of 6%, which is the half of the maximum compression strain (12%). Such a strain value permits the least extrapolation for stress analysis at each strain rate. Also, every stress-strain curve collected at three temperatures shows the obvious stress plateau above 4 to 5% strain, indicating that the strain from which the flow stresses is collected should be larger than 5% strain.

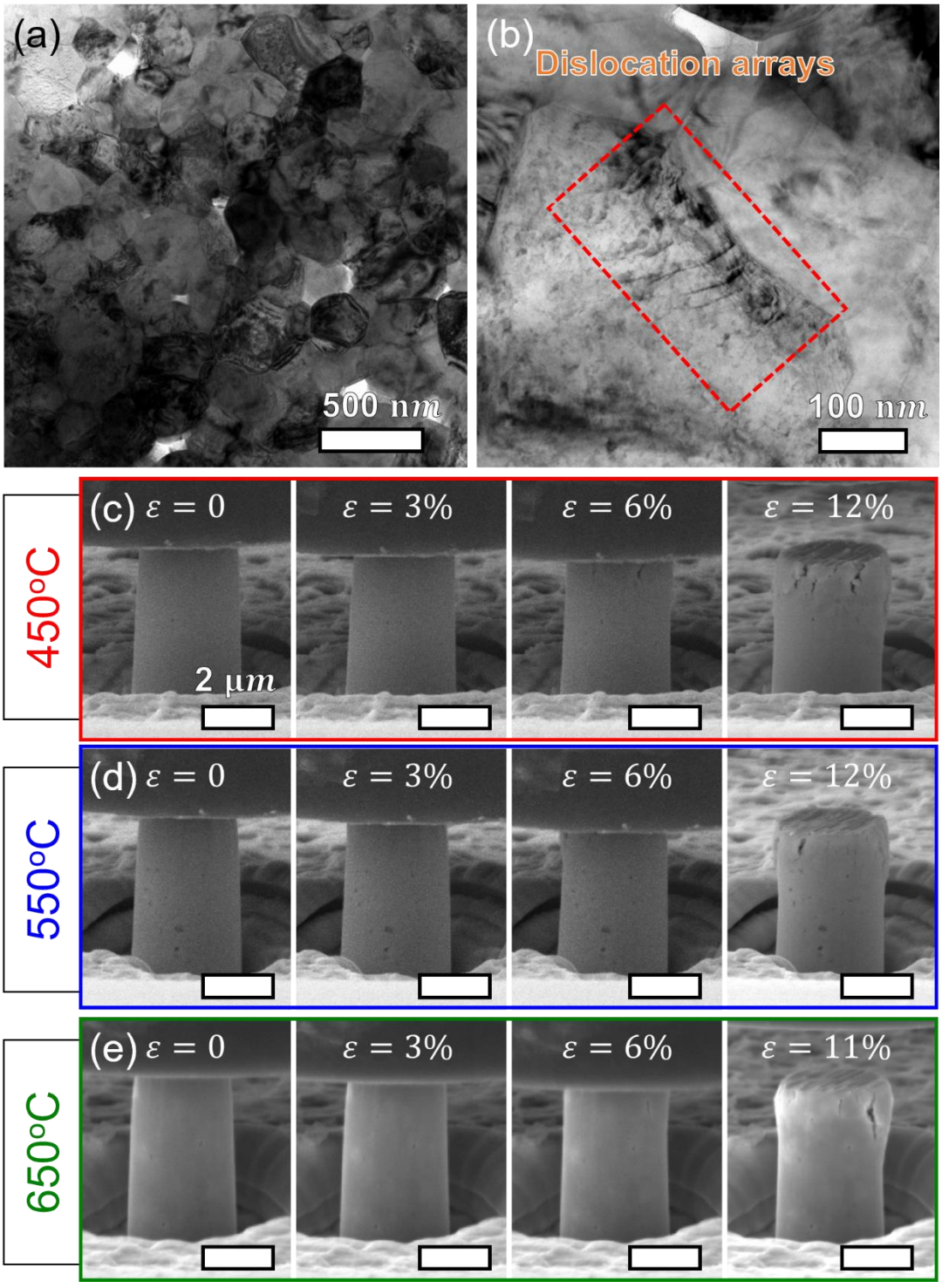

Figure 1. Microstructure and strain rate jump tests on the flash sintered 3YSZ. (a-b) Bright field TEM micrographs of the flash sintered 3YSZ showing (a) ultrafine grains and (b) an array of preexisting dislocations. (c-e) SEM snapshots of the pillars tested at 450, 550, and 650°C at 0, 3%,

6%, and final strains (11-12%). Several cracks propagated from the top surface of the pillar. Crack length and density reduce as test temperature rises.

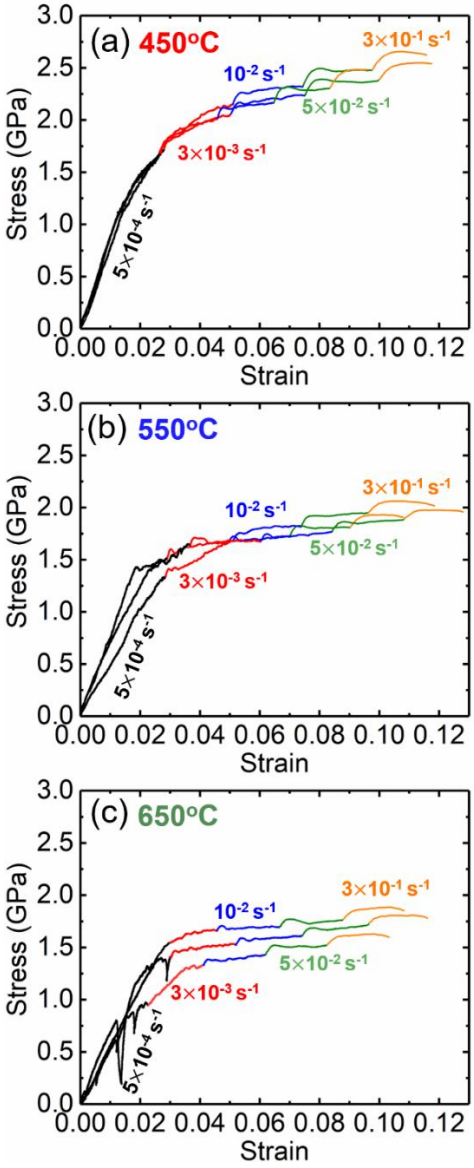

Figure 2. Stress-strain curves for strain rate jump tests on the flash sintered 3YSZ at 450, 550, and 650°C. Stress-strain curves for three strain rate jump tests at (a) 450°C, (b) 550°C, and (c) 650°C. Strain rate of 5×10^{-4} s^{-1} was employed in the elastic region. Strain rates of 3×10^{-3} s^{-1}, 1×10^{-2} s^{-1}, 5×10^{-2} s^{-1}, and 3×10^{-1} s^{-1} were utilized in the plastic region to obtain flow stresses at each temperature. The flow stresses increase with increasing strain rate and decreasing temperature.

The flow stresses at various temperatures and strain rates were extracted and plotted as a function of strain rate after taking natural logarithm (Figure S1 (a)). Strain rate sensitivity (m) at a fixed temperature and strain can be calculated by

$$m = \left(\frac{\partial ln\sigma}{\partial ln\dot{\varepsilon}}\right)_{\varepsilon,T} \quad (1),$$

where σ is an applied stress and $\dot{\varepsilon}$ is strain rate [22]. m values obtained from the slope of the fitting line in Figure S1 (a) at 450, 550, and 650 ^{o}C are 0.043$\pm$0.022, 0.034$\pm$0.011, and 0.030$\pm$0.030, respectively. The deformation mechanism of materials at elevated temperature follows an Arrhenius-type relation under the assumption that the deformation is dominated by a single process [23] and can be expressed by

$$\dot{\varepsilon} = A_o \sigma^n \exp\left(-\frac{Q}{RT}\right) \quad (2),$$

where A_o is the pre-exponential constant, n is the stress exponent, and Q is activation energy of the dominant deformation mechanism. When we assume the constant stress exponent and applied stress, Equation (2) can be rewritten as,

$$\dot{\varepsilon} = A_1 \exp\left(-\frac{Q}{RT}\right) \quad (3)$$

where A_1 is a constant, which includes the applied stress term [24]. The assumption of the constant stress exponent for the power law means that there is no transition in deformation mechanisms within the test temperatures. When the applied stress is fixed at 2,000 MPa, the corresponding strain rates can be obtained at each temperature by drawing a horizontal line in Figure S1 (a). By plotting ln$\dot{\varepsilon}$ vs. 1000/T, the activation energy can be calculated from the slope (Figure S1 (b)). The activation energy so calculated is 347 $\pm$151 kJ/mol. Plotting $\ln\left(\dot{\varepsilon}\exp\left(\frac{Q}{RT}\right)\right)$ vs. lnσ with a substitution of the activation energy of 347 kJ/mol into Equation (1) yields an unusually large

stress exponent of ~ 30 (Figure S1 (c)). The unphysically high stress exponent obtained using this method implies that threshold stresses must be taken into account for exploring the underlying deformation mechanism. The threshold stress, σ_o, can be graphically determined by plotting $\dot{\varepsilon}^{1/n}$ vs. σ at each temperature as follows:

$$\dot{\varepsilon} = A_o(\sigma - \sigma_o)^n \exp(-\frac{Q}{RT}) \quad (4)$$

The threshold stress is determined from the intercept between the linear regression of extrapolated data points and the stress axis (when $\dot{\varepsilon} = 0$) as demonstrated in Figure 3. To determine the threshold stress, the value of the stress exponent must be known. The most common deformation mechanisms of YSZ system are diffusional creep (n=1), grain boundary sliding (n=2) and dislocation creep (n=7) [25,26]. Figure 3 (a-c) shows $\dot{\varepsilon}^{1/n}$ vs. σ plot when we assume that the dominant deformation mechanism is diffusional creep, or grain boundary sliding, or dislocation creep, respectively. When the stress exponent is assumed to be 1, the fitting of data points significantly deviates from the linear regression dotted lines, indicating that n =1 is an unlikely scenario. Similarly, the assumption of n = 2 also leads to noticeable deviation from the linear regression line. When n = 7 is assumed, the linear regression lines exhibit best fits for data points at all three test temperatures, indicating that the same deformation mechanism takes place during this temperature range, which justifies the assumption of a constant stress exponent in Equation (3). Therefore, the threshold stresses at each temperature were obtained from the linear extrapolation of the experimental data using n = 7. The data was replotted in Figure 4 after taking the effective stress $(\sigma - \sigma_o)$ into account. Plotting $\ln(\sigma - \sigma_o)$ vs. $\ln\dot{\varepsilon}$ in Figure 4 (a) shows corrected strain rate sensitivities of 0.155±0.085, 0.142±0.050, and 0.154±0.151 at 450, 550, and 650^{o}C, respectively. The corrected activation energy of 145±74 kJ/mole was obtained at a constant

flow stress of 500 MPa by plotting $\ln\dot{\varepsilon}$ vs. 1000/T. The strain rate sensitivities become much greater and the activation energy significantly decrease after the correction of the flow stress. The determination of the threshold stresses with an imposed stress exponent of 7 naturally returns a self-consistent stress exponent of 6.7 as demonstrated in Figure 4 (c).

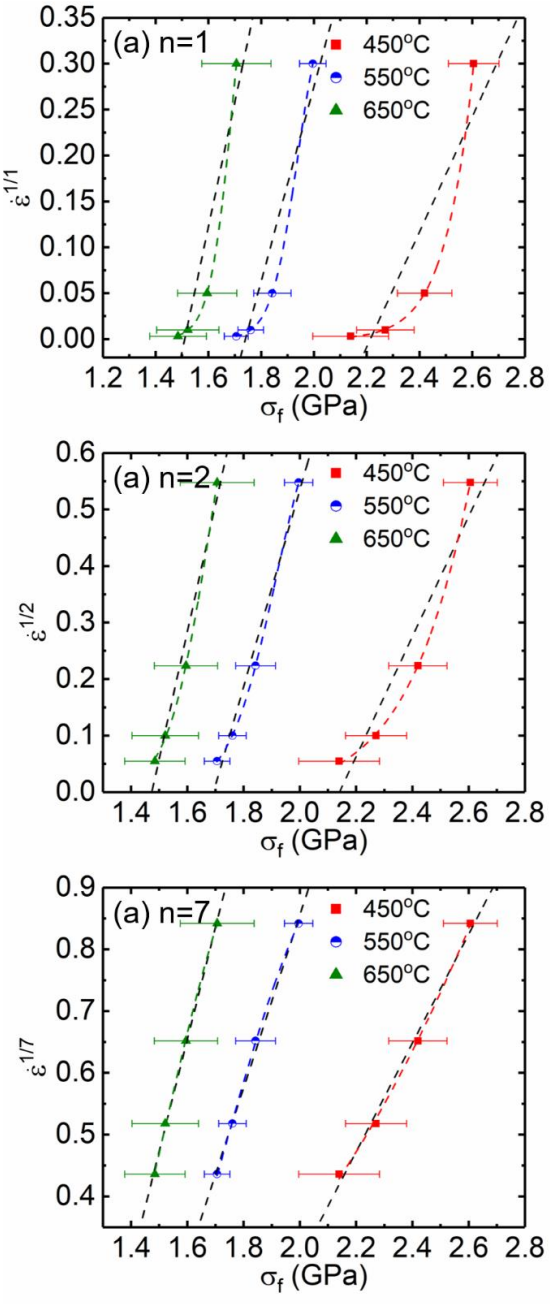

Figure 3. The determination of the threshold stress for the flash sintered 3YSZ at 450, 550, and 650^{o}C. (a) The determination of the threshold stress with a stress exponent of 1. The actual data points are significantly deviated from the linear regression lines as indicated by the curved dash lines. (b) The determination of the threshold stress with a stress exponent of 2. The actual data shows better linear fit than those with a stress exponent of 1, but still deviates from the linear regression lines by exhibiting positive upward curvature. (c) The determination of the threshold stress with a stress exponent of 7. The linear regression lines match well with the actual data. The extrapolation of the linear line to zero strain rate describes the threshold stress.

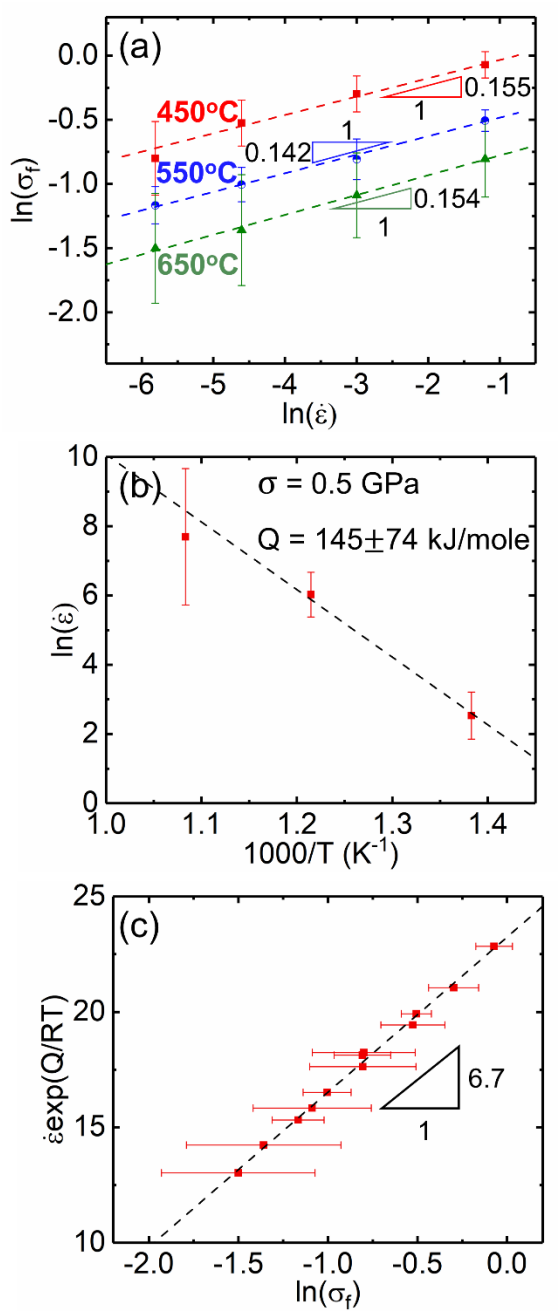

Figure 4. Corrected data processing from strain rate jump tests on the flash sintered 3YSZ at 450, 550, and 650ºC in consideration of the presence of the threshold stress. (a) The corrected flow stress as a function of strain rates at each temperature. The strain rate sensitivities after the correction increase to 0.15. (b) Temperature dependence of strain rate at a flow stress of 500 MPa. The activation energy is estimated to be 145±74 kJ/mole. (c) The corrected flow stress

versus the normalized strain rate. The data correction with an imposed stress exponent of 7 returns the stress exponent of 6.7.

4. Discussion

A majority of ceramic materials have little dislocations, unless deformed at high temperatures. Prior studies on the flash-sintered 3YSZ show that abundant grains of 3YSZ retain arrays of dislocations. Some dislocations exist near the triple junctions where the stress is concentrated during the flash sintering process [20]. This noticeable presence of high-density dislocations in the flash-sintered 3YSZ is surprising. It has been shown that flash sintering can induce significant amount of point defects in ceramics [19]. We anticipate that substantial mass transport during flash sintering, 4-5 orders of magnitude faster than conventional diffusion, results in considerable plastic flow, which is accommodated by generation and migration of a high-density of dislocations [3]. We also hypothesize that during flash sintering, the transient high current densities through specimens promote sintering and introduce a significant number of defects, such as Frenkel defects [2], dislocation loops, and stacking faults. The formation or nucleation of these defects facilitate the plastic deformation of flash sintered YSZ via a defect (dislocation) dominated plasticity. The activity of dislocations may not play a significant role in the deformability of 3YSZ at room temperature as the glide of dislocations is often hindered by the strong covalent and ionic bonding. However, the nucleation and activity of dislocations in bulk 3YSZ were often observed after mechanical tests at high temperatures (> 800^{o}C) [27,28]. In the current study, abundant intragranular dislocations and entanglement were already generated during the high strain rate mass flow in the flash-sintered specimens. Furthermore, the plastic deformation of ceramics by dislocation glide in micromechanical tests has been observed previously because the

miniaturization of specimen decreases strain gradients and the population of intrinsic flaws [29–31]. Therefore, it may be possible that the numerous preexisting dislocations contributes to the deformability of the flash-sintered 3YSZ at the intermediate test temperatures in the current study.

Initial plots of the experimental data from the strain rate jump tests, following Equation (1), yield the stress exponent of 30, too high to physically describe the appropriate deformation mechanisms. Such an abnormally large n value has been seen before, and the introduction of threshold stress as shown in Equation (4) returns a more appropriate n value and activation energy [32–34]. Following the similar methodology, the linear regression of the data using a n value of 7 provides the best linear fit as evidenced in Figure 3(c). Furthermore, the usage of modified creep equation returns a self-consistent n value of 6.7, indicating the methodology applied here is appropriate. n value of 7 corresponds to dislocation glide dominated creep mechanism. Thus, the current study suggest that the dislocation activity may be the dominant deformation mechanism in the flash-sintered 3YSZ over 450 ~ 650^{o}C. This temperature range is lower than the onset of dislocation controlled creep in conventional YSZ, typically much greater than 800^{o}C.

Table 1. Flow stress, yield strength and threshold stress at each temperature and strain rate.

Temperature (^{o}C)	Strain rate (s^{-1})	Flow stress (GPa)	Yield strength (GPa)	Threshold stress (GPa)
450	0.003	2.14±0.14	1.32±0.25	1.67±0.05
	0.01	2.27±0.11		
	0.05	2.42±0.10		
	0.3	2.61±0.10		
550	0.003	1.71±0.05	1.19±0.10	1.39±0.02
	0.01	1.76±0.05		
	0.05	1.84±0.07		
	0.3	2.00±0.05		
650	0.003	1.48±0.11	1.07±0.13	1.24±0.11
	0.01	1.52±0.12		
	0.05	1.60±0.11		
	0.3	1.71±0.13		

The threshold stresses obtained from the intercept of the linear extrapolation with the stress axis are 1.67, 1.39, 1.24 GPa for tests at 450, 550, and 650^{o}C, respectively. Higher temperature weakens the strong covalent and ionic bonding of 3YSZ, such that the threshold stress for dislocations to activate is mitigated as temperature increases. Furthermore, the calculated threshold stresses are somewhat comparable to the yield strength of specimens at each temperature as shown in Table 1. In general, yield strength of polycrystalline ceramic materials indicates the stress necessary for microcracking, phase transformation, or dislocation movement [35]. In addition, it was reported that dislocation dominated plastic flow is favorable at the low homologous temperature and high external stress [36]. The highest test temperature in this *in-situ* study is equivalent to $0.3T_m$ and the applied external stress is higher than 1 GPa. Aforementioned evidences, including abundant preexisting dislocations, best linear fit with n value of 7, and threshold stresses comparable to yield strengths, imply that the major deformation mechanism of the flash-sintered 3YSZ may be the dislocation creep over 450 - 650^{o}C.

Table 2. Activation energy of grain boundary and lattice diffusion for Zr, Y, O, and oxygen vacancy (V_o).

	Grain boundary diffusion (kJ/mole)	Lattice diffusion (kJ/mole)
Zr	310 [37]	390 [37]
Y	290 [37]	440 [37]
O	188 [38]	220 [38]
V_o	-	96.5 - 164 [39–42]

In addition, the activation energy for the rate controlling mechanism is ~145 kJ/mol after taking the presence of threshold stress into consideration. Such a value is less than the activation energy for grain boundary diffusion and lattice diffusion of Zr, Y, and O, but comparable to the activation energy for oxygen vacancy migration (96.5 ~ 164 kJ/mol) in YSZ (See Table 2) [39–42]. Dislocations activated by the external stress are often immobilized by point defects and/or grain boundaries, in which dislocation climb comes into play to retrigger dislocation movements. Abundant oxygen vacancies induced by flash sintering would diffuse through the lattice of YSZ for dislocation climb to occur. Therefore, the activation energy of 145 kJ/mol obtained from the strain rate jump tests may indicate that the rate controlling process in the flash-sintered 3YSZ at 450 ~ 650^{o}C is dislocation climb through the oxygen vacancy migration.

5. Conclusions

In summary, 3YSZ was processed by the flash sintering technique under an electric field of 150 V/cm. *In-situ* microcompression tests on the flash sintered 3YSZ was performed at 450 ~ 650^{o}C to study the underlying deformation mechanism. Strain rate jump tests lead to a stress exponent of ~ 7, and threshold stresses comparable to the yield strengths. The calculated activation energy of 145 kJ/mol is comparable to the activation energy for oxygen vacancy migration. This study suggests that the abundant defects induced during flash sintering (oxygen vacancies, and dislocation) lead to improved plasticity, and the deformation mechanism may be dislocation climb assisted by oxygen vacancy migration over the temperature range of 450 - 650^{o}C for the flash-sintered 3YSZ. This study sheds lights on the mechanical behavior of an important class of ceramic materials that have wide spread industrial applications.

Acknowledgement

This work is supported by the U.S. Office of Naval Research N00014-17-1-2087 (sample preparation and *in-situ* SEM), N0014-16-1-2778 (TEM) and partly by N0014-16-S-BA10. QL is supported by Department of Energy OBES (Grant No. DE-SC0016337). We also acknowledge access to Life Science Microscopy Facility and the microscopy center of School of Materials Engineering at Purdue University.

References

[1] Guillon O, Gonzalez-Julian J, Dargatz B, et al. Field-assisted sintering technology/spark plasma sintering: Mechanisms, materials, and technology developments. Adv. Eng. Mater. 2014;16:830–849.

[2] Cologna M, Rashkova B, Raj R. Flash sintering of nanograin zirconia in <5 s at 850°C. J. Am. Ceram. Soc. 2010;93:3556–3559.

[3] Jha SK, Terauds K, Lebrun J, et al. Beyond flash sintering in 3 mol % yttria stabilized zirconia. J. Ceram. Soc. Japan. 2016;124:283–288.

[4] Cologna M, Prette ALG, Raj R. Flash-sintering of cubic yttria-stabilized zirconia at 750°C for possible use in SOFC manufacturing. J. Am. Ceram. Soc. 2011;94:316–319.

[5] Jha SK, Raj R. The effect of electric field on sintering and electrical conductivity of Titania. J. Am. Ceram. Soc. 2014;97:527–534.

[6] Charalambous H, Jha SK, Lay RT, et al. Investigation of temperature approximation methods during flash sintering of ZnO. Ceram. Int. 2018;1–8.

[7] Li J, Guan L, Zhang W, et al. Sintering behavior of samarium doped ceria under DC electrical field. Ceram. Int. 2018;44:2470–2477.

[8] Padture NP. Thermal Barrier Coatings for Gas-Turbine Engine Applications. Science. 2012;280:280–285.

[9] Kelly JR, Denry I. Stabilized zirconia as a structural ceramic: An overview. Dent. Mater. 2008;24:289–298.

[10] Ramamoorthy R, Dutta PK, Akbar S a. Oxygen sensors : Materials , methods , designs. J. Mater. Sci. 2003;38:4271–4282.

[11] Tao S, Irvine JTS. A redox-stable efficient anode for solid-oxide fuel cells. Nat. Mater. 2003;2:320–323.

[12] Lai A, Du Z, Gan CL, et al. Shape Memory and Superelastic Ceramics at Small Scales. Science. 2013;341:1505–1508.

[13] Du Z, Zeng XM, Liu Q, et al. Size effects and shape memory properties in ZrO_2 ceramic micro- and nano-pillars. Scr. Mater. 2015;101:40–43.

[14] Zeng XM, Lai A, Gan CL, et al. Crystal orientation dependence of the stress-induced martensitic transformation in zirconia-based shape memory ceramics. Acta Mater. 2016;116:124–135.

[15] Camposilvan E, Anglada M. Size and plasticity effects in zirconia micropillars compression. Acta Mater. 2016;103:882–892.

[16] Zeng XM, Du Z, Schuh CA, et al. Microstructure, crystallization and shape memory behavior of titania and yttria co-doped zirconia. J. Eur. Ceram. Soc. 2016;36:1277–1283.

[17] Du Z, Zeng XM, Liu Q, et al. Superelasticity in micro-scale shape memory ceramic particles. Acta Mater. 2017;123:255–263.

[18] Cho J, Li J, Li Q, et al. In-situ high temperature micromechanical testing of ultrafine grained yttria-stabilized zirconia processed by spark plasma sintering. Acta Mater. 2018;155:128–137.

[19] Narayan J. A new mechanism for field-assisted processing and flash sintering of materials. Scr. Mater. 2013;69:107–111

[20] Cho J, Li Q, Wang H, et al. High temperature deformability of ductile flash sintered ceramics via in-situ compression. Nat. Commun. 2018;9:2063.

[21] Carpenter JS, Misra A, Uchic MD, et al. Strain rate sensitivity and activation volume of Cu/Ni metallic multilayer thin films measured via micropillar compression. Appl. Phys. Lett. 2012;101.

[22] Wei Q, Cheng S, Ramesh KT, et al. Effect of nanocrystalline and ultrafine grain sizes on the strain rate sensitivity and activation volume: Fcc versus bcc metals. Mater. Sci. Eng. A. 2004;381:71–79.

[23] Mukherjee AK. The Rate Controlling Mechanism in Superplasticity. Mater. Sci. Eng. 1971;8:83–89.

[24] Zhang X, Wang H, Scattergood RO, et al. Studies of deformation mechanisms in ultra-fine grained and nanostructured zinc. Acta mater. 2002;50:4823–4830.

[25] Balasubramanian N, Langdon TG. Flow processes in superplastic yttria-stabilized zirconia: A Deformation Limit Diagram. Mater. Sci. Eng. A. 2005;409:46–51.

[26] Charit I, Chokshi AH. Experimental evidence for diffusion creep in the superplastic 3 mol% yttria-stabilized tetragonal zirconia. Acta Mater. 2001;49:2239–2249.

[27] Morita K, Hiraga K. Reply to "comment on the role of intragranular dislocations in superplastic yttria-stabilized zirconia." Scr. Mater. 2003;48:1402–1407.

[28] Morita K, Hiraga K. Deformed substructures in fine-grained tetragonal zirconia. Philos. Mag. Lett. 2001;81:311–319.

[29] Korte S, Barnard JS, Stearn RJ, et al. Deformation of silicon - Insights from microcompression testing at 25-500 ^{o}C. Int. J. Plast. 2011;27:1853–1866

[30] Montagne A, Pathak S, Maeder X, et al. Plasticity and fracture of sapphire at room temperature: Load-controlled microcompression of four different orientations. Ceram. Int. 2014;40:2083–2090.

[31] Kiani S, Leung KWK, Radmilovic V, et al. Dislocation glide-controlled room-temperature plasticity in 6H-SiC single crystals. Acta Mater. 2014;80:400–406.

[32] Mishra RS, Mukherjee AK. On superplasticity in silicon carbide reinforced aluminum composites. Scr. Metall. Mater. 1991;25:271–275.

[33] Mishra, R.S., Bieler, T.R., Mukherjee AK. On the superplastic behaviour of mechanically alloyed aluminum alloys. Scr. Metall. Mater. 1992;26:1605–1608.

[34] Mishra, R.S., Bieler, T.R., Mukherjee AK. Superplasticity in powder metallurgy aluminum alloys and composites. Acta Metall. Mater. 1995;43:877–891.

[35] Lankford J, Predebon WW, Staehler JM, et al. The role of plasticity as a limiting factor in the compressive failure of high strength ceramics. Mech. Mater. 1998;29:205–218.

[36] Ashby MF, Verrall RA. Diffusion-accommodated flow and superplasticity. Acta Metall. 1973;21:149–163.

[37] Sakka Y, Oishi Y, Ando K. Zr-Hf interdiffusion in polycrystalline Y_2O_3-$(Zr+Hf)O_2$. J. Mater. Sci. 1982;17:3101–3105.

[38] Brossmann U, Knöner G, Schaefer HE, et al. Oxygen diffusion in nanocrystalline ZrO_2. Rev. Adv. Mater. Sci. 2004;6:7–11.

[39] Wakiya N, Tajiri N, Kiguchi T, et al. Activation energy of oxygen vacancy diffusion of yttria-stabilized-zirconia thin film determined from DC current measurements below 150^{o}C. Japanese J. Appl. Physics, Part 2 Lett. 2006;45.

[40] Dong Y, Chen I. Onset Criterion for Flash Sintering. J. Am. Ceram. Soc. 2015;3627:3624–3627.

[41] Todd RI, Bonilla RS, Sneddon T, et al. Electrical characteristics of flash sintering : thermal runaway of Joule heating. J. Eur. Ceram. Soc. 2015;35:1865–1877.

[42] Ramamoorthy R, Sundararaman D, Ramasamy S. Ionic conductivity studies of ultrafine-grained yttria stabilized zirconia polymorphs. Solid State Ionics. 1999;123:271–278.